Journal of Molecular Catalysis A: Chemical xxx (2013) xxx–xxx

Contents lists available at ScienceDirect

Journal of Molecular Catalysis A: Chemical

journal homepage: www.elsevier.com/locate/molcata

Promoting effect of Ru on Ir-ReO_x/SiO_2 catalyst in hydrogenolysis of glycerol

Masazumi Tamura, Yasushi Amada, Sibao Liu, Zhenle Yuan, Yoshinao Nakagawa, Keiichi Tomishige*

Graduate School of Engineering, Tohoku University, Aoba 6-6-07, Aramaki, Aoba-ku, Sendai 980-8579, Japan

ARTICLE INFO

Article history:
Received 5 June 2013
Received in revised form 18 August 2013
Accepted 11 September 2013
Available online xxx

Keywords:
Hydrogenolysis
Glycerol
1,3-Propanediol
1-Propanol

ABSTRACT

Ru-added Ir-ReO_x/SiO_2 catalysts worked as efficient catalysts for the selective hydrogenolysis of glycerol to 1,3-propanediol and 1-propanol. 0.9 wt% Ru-added Ir-ReO_x/SiO_2 catalyst demonstrated high activity for the hydrogenolysis of glycerol to 1,3-propanediol with high selectivity comparative to Ir-ReO_x/SiO_2. In addition, 4.4 wt% Ru-added Ir-ReO_x/SiO_2 catalyst with H_2SO_4aq showed high activity for the selective hydrogenolysis of glycerol to 1-propanol, and the yields of 1-propanol and total propanols (1-propanol + 2-propanol) were 71% and 84%, respectively. On the basis of various analyses such as TPR (temperature-programmed reduction), XRD, XAFS and CO adsorption, the structure and reaction mechanism of Ru-added Ir-ReO_x/SiO_2 catalysts were proposed.

1. Introduction

Transformation of biomass and biomass-derived chemicals to value-added ones attracts much attention from the viewpoints of sustainable and environmentally friendly society [1–4]. Increasing biodiesel production by transesterification of plant oils and animal fats affords a large amount of glycerol as a byproduct [5–7]. Therefore, to establish various new methods for converting glycerol to various valuable chemicals is duty of chemistry. Transformation processes of glycerol include fermentation, oxidation, reduction, dehydration, gasification, carboxylation, esterification and so on [5–8]. Among these processes, hydrogenolysis of glycerol to 1,2-propanediol [9–25], 1,3-propanediol [24,26–44], 1-propanol [42,45] and propane [46] is promising because these products are very important for polymer, cosmetics, pharmaceuticals, solvents, and so on. From the environmental and practical viewpoints such as catalyst reusability, handling and product separation, heterogeneous catalysts have been widely developed to transform glycerol into the above chemicals. In particular, catalytic hydrogenolysis process to 1,3-propanediol (Scheme 1) is an important route because of the highest value in the hydrogenolysis products of glycerol. In the previous reports, different metal based catalysts such as supported Cu [29], Rh [24,26,37], Pt [25,27,28,30–32,35,36,40,41,44], Ir [33,34,38,39] catalysts have been applied, and Arundhathi and co-workers reported that Pt/WO_x/AlOOH was effective for the reaction to give the highest 1,3-propanediol yield (69%) [45].

In our previous reports, we demonstrated that metal oxide-modified supported metal catalysts (MO_x-modified-Metal catalysts) such as Ir-ReO_x [33,34,38,39], Rh-ReO_x [24,37] and Rh-MoO_x [37] catalysts were effective for the hydrogenolysis of glycerol to 1,3-propanediol. In particular, Ir-ReO_x/SiO_2 catalyst is one of the best catalysts for this reaction to provide high initial selectivity (~70%) and yield of 1,3-propanediol (38%). On the other hand, the hydrogenolysis of glycerol to 1-propanol, which has been produced industrially through hydroformylation of ethylene, was also reported in our laboratory, and the high yield of 76% 1-propanol in 24 h was accomplished over Rh-ReO_x/SiO_2 catalyst [44]. As above, various effective catalyst systems for 1,3-propanediol and 1-propanol have been developed, however, from the industrial viewpoint, higher activity for selective hydrogenolysis of glycerol as well as high selectivity is required.

Modification of supported metal catalysts with various species brings about many good or bad effects on the catalyst performance and stability [47–57]. Non-metals additives such as Na and S have been reported to be effective to control the electronic state of main catalytic species [47–51], resulting in change of its catalyst function. On the other hand, addition of transition metals to noble metal supported catalysts can modify the property of the noble metals, leading to drastic change of activity and selectivity for various reactions [24,33,34,37–39,44,52–57]. The mechanism

* Corresponding author. Tel.: +81 22 795 7214; fax: +81 22 795 7214.
E-mail addresses: tomi@erec.che.tohoku.ac.jp, tomi@tulip.sannet.ne.jp (K. Tomishige).

1381-1169/$ – see front matter © 2013 Elsevier B.V. All rights reserved.
http://dx.doi.org/10.1016/j.molcata.2013.09.015

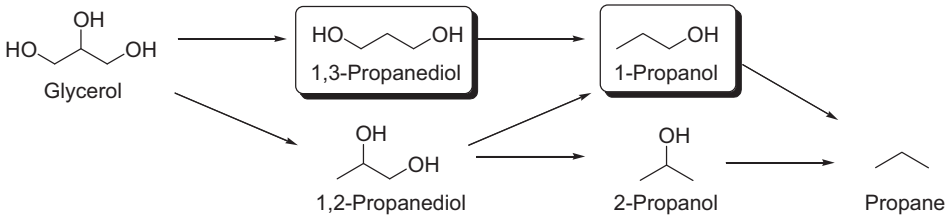

Scheme 1. Hydrogenolysis of glycerol.

of these performance changes includes the control of the electron density of the noble metal [52–55], cover of the unfavorable sites on the noble metal [54–57], cooperation of additive metal species with the noble metal [24,33,34,37–39,44,55,56], and control of the noble metal structure [24,33,34,37–39,53–55,57]. Therefore, it is important to investigate the further modification effect on 'MO_x-modified-Metal catalysts' for the breakthrough in the heterogeneous catalyst design.

In this report, Ir-ReO_x/SiO_2 catalyst was modified with various transition metals (Cu, Ni, Ag, Co, Zn, Ru, Rh and Pd), acidic additives (S, P and B), and basic ion (Na). Among these catalysts, Ru-added Ir-ReO_x/SiO_2 catalysts showed the highest activity for the hydrogenolysis of glycerol. In addition, on the basis of TPR, XRD, EXAFS and CO adsorption, the reaction mechanism over Ru-modified Ir-ReO_x/SiO_2 catalyst and the catalyst structure will be discussed.

2. Experimental

The SiO_2 (G-6, BET surface area 535 m^2/g) supplied by Fuji Silysia Chemical Ltd. was used as a support of the catalysts. M/SiO_2 (M = Rh, Ru, Pd, Ni, Co, Zn, Cu and Ag) catalysts and Ir/SiO_2 were prepared by impregnating SiO_2 with H_2IrCl_6 (Furuya Metals Co., Ltd.), $RhCl_3{\cdot}3H_2O$ (Soekawa Chemical Co., Ltd.), $RuCl_3{\cdot}nH_2O$ (Kanto Chemical Co., Ltd.) and $PdCl_2$ (Kanto Chemical Co., Ltd.), $Cu(NO_3)_2{\cdot}3H_2O$ (Fluka Chemical Co., Ltd.), $Co(NO_3)_2{\cdot}6H_2O$ (Wako Pure Chemical Industries, Ltd.), $Zn(NO_3)_2{\cdot}6H_2O$ (Wako Pure Chemical Industries, Ltd.), $Ni(NO_3)_2{\cdot}6H_2O$ (Wako Pure Chemical Industries, Ltd.) and $AgNO_3$ (Wako Pure Chemical Industries, Ltd.). After evaporating the solvent and drying at 383 K for 12 h, they were calcined in air at 773 K for 3 h. M-Ir/SiO_2 (M = Rh, Ru, Pd, Ni, Co, Zn, Cu and Ag) were prepared by impregnating M/SiO_2 after the calcination procedure with H_2IrCl_6 (Furuya Metals Co., Ltd.), and then the solvent was evaporated and dried at 383 K for 12 h. M-Ir-ReO_x/SiO_2 (Rh, Ru, Pd, Ni, Co, Zn, Cu and Ag) were prepared by impregnating M-Ir/SiO_2 after the drying procedure with aqueous solutions of NH_4ReO_4 (Soekawa Chemical Co., Ltd.). These catalysts were calcined in air at 773 K for 3 h after drying at 383 K for 12 h. This preparation method of catalysts is defined as method (A). The loading amounts of Ir and Re were 4.0 and 7.7 wt%, respectively (Re/Ir molar ratio = 2), and that of additive was represented by the weight% of the additives to the total catalyst in parenthesis like M(X)-Ir-ReO_x/SiO_2. M-Ir-ReO_x/SiO_2 (M = Na, P, B, S) were prepared by impregnating Ir-ReO_x/SiO_2 prepared as above with $(NH_4)_2SO_4$ (Wako Pure Chemical Industries, Ltd.), Na_2CO_3 (Wako Pure Chemical Industries, Ltd.), $(NH_4)_2HPO_4$ (Wako Pure Chemical Industries, Ltd.) and $(NH_4)_2B_4O_7\ 4H_2O$ (Kanto Chemical Co., Ltd.). After evaporating the solvent and drying at 383 K for 12 h, they were calcined in air at 773 K for 3 h. This preparation method of catalysts is defined as method (B). Ru(1)-Ir-ReO_x/SiO_2 and Ru(0.1)-Ir-ReO_x/SiO_2 were also prepared by method (B). The catalysts prepared by the method (B) were denoted as M-Ir-ReO_x/SiO_2 (B) (M = Rh, Ru, Pd, Ni, Co, Zn, Cu, Ag, P, S, B and Na) and the catalysts were prepared by the method (A) unless denoted.

2.1. Activity tests

Activity tests were performed in a 190-ml stainless steel autoclave with an inserted glass vessel. The catalyst was put into an autoclave together with a spinner and an appropriate amount of water and heated at 473 K with 8 MPa H_2 for 1 h for the reduction pretreatments. After the pretreatment, the autoclave was cooled down, and hydrogen was removed. Glycerol (Wako Pure Chemical Industries, Ltd., >99%) was put into the autoclave together with sulfuric acid (Wako Pure Chemical Industries, Ltd.) diluted with water. After sealing the reactor, the air content was purged by flushing thrice with 1 MPa hydrogen (99.99%; Nippon Peroxide Co., Ltd.). The autoclave was then heated to 393 K, and the temperature was monitored using a thermocouple inserted in the autoclave. After the temperature reached 393 K, the H_2 pressure was increased to 8 MPa. During the experiment, the stirring rate was fixed at 250 rpm (magnetic stirring). After an appropriate reaction time, the reactor was cooled down and the gases were collected in a gas bag. The autoclave contents were transferred to a vial, and the catalyst was separated by centrifugation and filtration. The standard conditions for the reaction were as follows: 393 K reaction temperature, 8.0 MPa initial hydrogen pressure, 4 h reaction time, 4 g glycerol, 2 g water, 1.5 mg H_2SO_4 ($H^+/Ir = 1$) and 150 mg supported metal catalyst. The parameters were changed appropriately in order to investigate the effect of reaction conditions. Details of the reaction conditions are described in each result. The products were analyzed using a gas chromatograph (Shimadzu GC-2014 and GC-17A) equipped with FID. A TC-WAX capillary column (diameter 0.25 mm i.d., 30 m) was used for the separation. Products were also identified using GC-MS (QP5050, Shimadzu). The products in the glycerol hydrogenolysis were 1,3-propanediol (1,3-PrD), 1,2-propanediol (1,2-PrD), 1-propanol (1-PrOH), 2-propanol (2-PrOH) and propane. In addition, the degradation products such as ethyleneglycol, ethanol, ethane and methane were detected. The conversion and the selectivity were defined on the carbon basis in the similar way as reported previously [19,20]. The mass balance was also confirmed in each result and the difference in mass balance was always in the range of the experimental error. The agreement in terms of the mass balance indicated that polymeric by-products were not formed (±10%). The used catalyst was collected by centrifugation. The collected catalyst was washed with excess water and dried in air, and then calcined at 773 K at 3 h. A slight loss (<10% in weight) was observed during the recovery process and was compensated with fresh catalyst in each reuse experiment.

2.2. Catalyst characterization

Temperature-programmed reduction (TPR) was carried out in a fixed-bed reactor equipped with a thermal conductivity detector using 5% H_2 diluted with Ar (30 ml/min). The amount of catalyst was 0.05 g, and temperature was increased from room temperature to 1123 K at a heating rate of 10 K/min. X-ray diffraction (XRD) patterns were recorded by a diffractometer (Rigaku Ultima). Average metal particle size was estimated using the Scherrer equation

[58]. The amount of CO chemisorption was measured in a high-vacuum system using a volumetric method (Micrometrics ASAP 2020). Before adsorption measurements, the catalysts were treated in H_2 at 473 K for 1 h. Subsequently the adsorption was performed at room temperature. Gas pressure at adsorption equilibrium, the sample weight and the dead volume of the apparatus was about 1.1 kPa, 0.1 g and 8 cm^3, respectively.

The extended X-ray absorption fine structure (EXAFS) spectra were measured at the BL01B1 station at SPring-8 with the approval of the Japan Synchrotron Radiation Research Institute (JASRI; Proposal No. 2013A1048). The storage ring was operated at 8 GeV, and a Si (1 1 1) single crystal was used to obtain a monochromatic X-ray beam. Two ion chambers for I_0 and I were filled with 85% N_2 + 15% Ar and 50% N_2 + 50% Ar, respectively, for Re L_3-edge and Ir L_3-edge measurements, and 100% Ar and 100% Ar for Ru K-edge measurement. We prepared the sample after the catalytic use as follows. The catalytic reaction was carried out in an autoclave. The standard reaction conditions were the same as in activity tests. After cooling, the wet catalyst powder was transferred to the measurement cell in a glove bag filled with nitrogen. The thickness of the cell filled with the powder was 2 mm to give an edge jump of 0.6, 0.4 and 0.6 for Ir L_3-edge, Re L_3-edge and Ru K-edge measurement, respectively. The EXAFS data were collected in a transmission mode. For EXAFS analysis, the oscillation was first extracted from the EXAFS data using a spline smoothing method [59]. Fourier transformation of the k^3-weighted EXAFS oscillation from the k space to the r space was performed to obtain a radial distribution function. The inversely Fourier filtered data were analyzed using a usual curve fitting method [60,61]. For curve fitting analysis, the empirical phase shift and amplitude functions for the Re—O and Ir—Ir bonds were extracted from data for NH_4ReO_4 and Ir metal, respectively. The empirical phase shift and amplitude functions for Ru—Ru bond were extracted from data of Rh foil, because the quality of our Ru powder was so low that it could not be used as a reference compound. Theoretical functions for the Re—Ir, Re—Ru and Ru—Re bond were calculated using the FEFF8.2 program [62]. The Re—Ir and Ir—Ir bonds are represented by the Re-Ir (or -Re) and Ir-Ir (or -Re) in the curve fitting results. This is because it is very difficult to distinguish between Ir and Re as a scattering atom. Analyses of EXAFS data were performed using a computer program (REX2000, ver. 2.5.9; Rigaku Corp.). Error bars for each parameter were estimated by stepping each parameter, while optimizing the others parameter, until the residual factor becomes two times as its minimum value [63].

3. Results and discussion

3.1. Additive effect on Ir-ReO_x/SiO_2 for the hydrogenolysis of glycerol to 1,3-propanediol

At first, the additive effect of S, P, B or Na was examined for the hydrogenolysis of glycerol. Table 1 shows the catalytic performances over Ir-ReO_x/SiO_2 catalysts modified with 0.1 or 1 wt% Na, S, P and B. For the catalysts with the addition of the acidic components (Table 1, entries 2–7), conversion and selectivity for 1,3-propanediol were similar to those of Ir-ReO_x/SiO_2 (Table 1, entry 1), which suggests that acidic additives have no influences on the active sites of Ir-ReO_x/SiO_2. However, as for Na-Ir-ReO_x/SiO_2 catalysts (Table 1, entries 8 and 9), negative effect on the activity was observed and in the case of Na(1)-Ir-ReO_x/SiO_2 the hydrogenolysis activity was completely lost. TPR profiles of Na-added Ir-ReO_x/SiO_2 catalysts were examined (Fig. S1). New peaks due to the reduction of IrO_2 or ReO_x were observed at higher temperature and the tendency is remarkable on Na(1)-Ir-ReO_x/SiO_2. This result indicates that addition of Na makes ReO_x or IrO_2 species hard to be reduced. Moreover, in the reaction of glycerol hydrogenolysis over Ir-ReO_x/SiO_2, addition of basic metal oxides such as MgO or CeO_2 to the reaction mixture resulted in much decrease of the activity [38], and addition of NaOH resulted in no activity (no shown data). Therefore, basic species will not only increase the reduction temperature of the catalyst but also poison the active sites of Ir-ReO_x/SiO_2, leading to the reduction of the activity.

Next, additions of various transition metals were tested for the hydrogenolysis of glycerol as shown in Table 2. Ni, Co, Zn and Cu-added Ir-ReO_x/SiO_2 catalysts (Table 2, entries 3–6) hardly showed the activity, and Ag-added Ir-ReO_x/SiO_2 (Table 2, entry 7) also provided lower conversion than Ir-ReO_x/SiO_2. In contrast, Pd-added Ir-ReO_x/SiO_2 catalysts showed similar conversion to Ir-ReO_x/SiO_2, although the selectivity of these catalysts was similar to or a little lower than that of Ir-ReO_x/SiO_2 (Table 2, entry 8). Surprisingly, in the case of Rh and Ru-added Ir-ReO_x/SiO_2 catalysts (Table 2, entries 9 and 11), about twice higher conversion than that of Ir-ReO_x/SiO_2 was observed with comparatively high selectivity (52, 54%), which is almost the same as that of Ir-ReO_x/SiO_2 (~60%) at the same conversion [33]. These results show that Ru and Rh metals are effective for the increase of hydrogenolysis activity without significant loss of selectivity to 1,3-propanediol. The reactions at longer time of 24 h were carried out using Ir-ReO_x/SiO_2, Ru(0.9)-Ir-ReO_x/SiO_2 and Rh(0.9)-Ir-ReO_x/SiO_2 (Table 2, entries 2, 10 and 12). Conversions over Ru(0.9)-Ir-ReO_x/SiO_2 and Rh(0.9)-Ir-ReO_x/SiO_2 catalysts were clearly higher than that over Ir-ReO_x/SiO_2. 1,3-Propanediol was obtained in 30% yield over Ru(0.9)-ReO_x/SiO_2 (Table 2, entry 10). From the viewpoints of activity, selectivity and price of metal, Ru-added Ir-ReO_x/SiO_2 is selected as a better catalyst for the selective hydrogenolysis of glycerol.

Table 3 shows the results of amount effect of Ru metal over Ir-ReO_x/SiO_2. Ru(4)/SiO_2 hardly showed activity (Table 3, entry 2). Regarding that the activity of Ir-ReO_x/SiO_2 was increased by addition of Ru species, synergy effect between Ru and Ir-ReO_x will enhance the activity. The effect of preparation methods on the catalytic performance of Ru-Ir-ReO_x/SiO_2 was tested using different methods (A) and (B) (Table 3, entries 3 and 4). Almost the same conversion and selectivity were obtained, which indicates that the catalytic performance is not influenced by the preparation method significantly. In the case that loading amount of Ru was 0.1 wt% (Table 3, entry 5), positive effect was hardly obtained. On the other hand, Ru(4.4)-Ir-ReO_x/SiO_2 catalyst showed five times as high conversion as Ir-ReO_x/SiO_2 with moderate selectivity (38.5%), which is lower than that of Ir-ReO_x/SiO_2 (~60%) at the same conversion [33]. Taking into account that selectivity of 1-propanol is comparatively high (36%), over-hydrogenolysis of 1,3-propanediol to 1-propanol will be accelerated as well as hydrogenolysis of glycerol to 1,3-propanediol, leading to low selectivity of 1,3-propanediol and high selectivity of 1-propanol.

3.2. Hydrogenolysis of glycerol to 1-propanol by Ru-added Ir-ReO_x/SiO_2 catalyst

As mentioned in Section 1, 1-propanol is also an attractive target in the hydrogenolysis of glycerol because it is produced from petrochemical-based materials. The synthesis route of 1-propanol from glycerol can be divided into two routes as follows (Scheme 1): (1) glycerol → 1,2-propanediol → 1-propanol and (2) glycerol → 1,3-propanediol → 1-propanol. If selective synthesis of 1,3-propanediol from glycerol is possible, the route (2) is more advantageous than the route (1) because hydrogenolysis of 1,3-propanediol provides only 1-propanol. As mentioned in the previous chapter, Ru(4.4)-Ir-ReO_x/SiO_2 can be expected as a feasible catalyst for the highly selective synthesis of 1-propanol from glycerol because of high activity for over-hydrogenolysis of 1,3-propanediol to 1-propanol. Table 4 shows the results of selective

Table 1
Glycerol hydrogenolysis over modified Ir-ReO_x/SiO_2.

Entry	Catalyst	Conv. (%)	Yield (1,3-PrD) (%)	Selectivity (%)				
				1,3-PrD	1,2-PrD	1-PrOH	2-PrOH	Others
1	Ir-ReO_x/SiO_2	9.4	6.2	66.2	11.9	15.8	5.6	0.5
2	S(0.1)-Ir-ReO_x/SiO_2 (B)	8.0	5.3	66.5	11.1	16.3	5.6	0.4
3	S(1)-Ir-ReO_x/SiO_2 (B)	8.6	5.7	66.6	10.8	16.5	5.8	0.4
4	P(0.1)-Ir-ReO_x/SiO_2 (B)	9.7	6.5	66.8	10.0	17.6	5.2	0.4
5	P(1)-Ir-ReO_x/SiO_2 (B)	5.2	3.0	58.2	12.2	24.2	4.9	0.5
6	B(0.1)-Ir-ReO_x/SiO_2 (B)	6.3	4.1	64.8	13.5	16.1	5.4	0.3
7	B(1)-Ir-ReO_x/SiO_2 (B)	8.5	5.7	67.2	11.3	15.8	5.5	0.3
8	Na(0.1)-Ir-ReO_x/SiO_2 (B)	5.6	3.4	61.6	18.1	13.5	6.3	0.5
9	Na(1)-Ir-ReO_x/SiO_2 (B)	0.3	0.0	0.0	83.0	10.2	6.6	0.2

Reaction conditions: glycerol 4 g, H_2O 2 g, catalyst 150 mg, P_{H_2} = 8 MPa (at 393 K), T = 393 K, t = 4 h. Reduction conditions: P_{H_2} = 8 MPa (at 473 K), T = 473 K, t = 1 h. PrD: propanediol; PrOH: propanol; Others: ethyleneglycol + ethanol + propane + ethane + methane.

hydrogenolysis of glycerol to 1-propanol. Since acid is known to promote the activity of Ir-ReO_x/SiO_2 for the selective hydrogenolysis of glycerol to 1,3-propanol [38], effect of H_2SO_4aq addition to Ru(4.4)-Ir-ReO_x/SiO_2 was investigated. The reaction was promoted by addition of H_2SO_4aq to Ru(4.4)-Ir-ReO_x/SiO_2, affording higher conversion than Ru(4.4)-Ir-ReO_x/SiO_2 alone without loss of selectivity of 1,3-propanediol + 1-propanol (Table 4, entries 1 and 2). This result indicates that addition of H_2SO_4aq is effective for raising the catalytic activity of Ru(4.4)-Ir-ReO_x/SiO_2. Ir-ReO_x/SiO_2, Ru(5)/SiO_2 and physically mixed catalyst composed of Ir-ReO_x/SiO_2 and Ru(5)/SiO_2 were examined for glycerol hydrogenolysis in the presence of H_2SO_4aq (Table 4, entries 3–5). Ru(5)/SiO_2 showed very low conversion even in the presence of H_2SO_4aq, and Ir-ReO_x/SiO_2 also presented lower conversion than Ru(4.4)-Ir-ReO_x/SiO_2 (Table 4,

Table 2
Glycerol hydrogenolysis over transition metal-added Ir-ReO_x/SiO_2.

Entry	Catalyst	t (h)	Conv. (%)	Yield (1,3-PrD) (%)	Selectivity (%)				
					1,3-PrD	1,2-PrD	1-PrOH	2-PrOH	Others
1	Ir-ReO_x/SiO_2	4	9.4	6.2	66.2	11.9	15.8	5.6	0.5
2		24	38.6	22.8	59.0	9.4	24.4	7.0	0.2
3	Ni(0.9)-Ir-ReO_x/SiO_2	4	0.0	0.0	0.0	0.0	0.0	0.0	0.0
4	Co(0.9)-Ir-ReO_x/SiO_2	4	0.3	0.0	3.2	75.8	16.6	3.1	1.3
5	Zn(0.9)-Ir-ReO_x/SiO_2	4	0.6	0.0	3.7	78.5	13.3	3.4	0.0
6	Cu(0.9)-Ir-ReO_x/SiO_2	4	1.4	0.4	26.7	47.2	17.1	8.2	0.8
7	Ag(0.9)-Ir-ReO_x/SiO_2	4	4.5	2.9	64.8	14.5	13.9	6.3	0.0
8	Pd(0.9)-Ir-ReO_x/SiO_2	4	9.0	4.5	50.0	32.1	12.4	5.2	0.4
9	Ru(0.9)-Ir-ReO_x/SiO_2	4	22.9	12.4	54.2	17.8	19.2	7.5	1.3
10		24	77.9	30.3	38.9	6.0	43.7	9.7	1.7
11	Rh(0.9)-Ir-ReO_x/SiO_2	4	19.4	10.1	51.9	21.3	20.3	6.2	0.3
12		24	65.8	24.3	36.9	14.4	39.6	8.5	0.5

Reaction conditions: glycerol 4 g, H_2O 2 g, catalyst 150 mg, P_{H_2} = 8 MPa (at 393 K), T = 393 K. Reduction conditions: P_{H_2} = 8 MPa (at 473 K), T = 473 K, t = 1 h. PrD: propanediol; PrOH: propanol; Others: ethyleneglycol + ethanol + propane + ethane + methane.

Table 3
Effect of Ru metal for hydrogenolysis of glycerol.

Entry	Catalyst	Ru/Ir ratio	Conv. (%)	Yield (1-PrOH) (%)	Selectivity (%)				
					1,3-PrD	1,2-PrD	1-PrOH	2-PrOH	Others
1	Ir-ReO_x/SiO_2	0.0	9.4	1.5	66.2	11.9	15.8	5.6	0.5
2	Ru(4)/SiO_2	–	1.5	0.3	8.2	23.3	20.9	2.7	39.0
3	Ru(0.9)-Ir-ReO_x/SiO_2	0.23	22.9	4.4	54.2	17.8	19.2	7.5	1.3
4	Ru(1)-Ir-ReO_x/SiO_2 (B)	0.25	28.3	6.7	52.9	15.9	23.7	6.8	0.7
5	Ru(0.1)-Ir-ReO_x/SiO_2 (B)	0.025	11.3	1.8	67.8	10.1	16.2	5.6	0.3
6	Ru(4.4)-Ir-ReO_x/SiO_2	1.1	44.6	16	38.5	16.0	36.0	7.1	2.4

Reaction conditions: glycerol 4 g, H_2O 2 g, catalyst 150 mg, P_{H_2} = 8 MPa (at 393 K), T = 393 K, t = 4 h. Reduction conditions: P_{H_2} = 8 MPa (at 473 K), T = 473 K, t = 1 h. PrD: propanediol; PrOH: propanol; Others: ethyleneglycol + ethanol + propane + ethane + methane.

Table 4
Results of hydrogenolysis of glycerol over various catalysts with or without H_2SO_4.

Entry	Catalyst	H_2SO_4	Conv. (%)	Yield (1,3-PrD) (%)	Selectivity (%)				
					1,3-PrD	1,2-PrD	1-PrOH	2-PrOH	Others
1	Ru(4.4)-Ir-ReO_x/SiO_2	None	44.6	17	38.5	16.0	36.0	7.1	2.4
2	Ru(4.4)-Ir-ReO_x/SiO_2	H^+/Ir = 1	60.7	20	33.7	11.7	43.0	6.8	4.9
3	Ir-ReO_x/SiO_2	H^+/Ir = 1	23.0	13	57.7	7.9	27.0	6.8	0.7
4	Ru(5)/SiO_2	H^+/Ir = 1	9.3	0.8	9.1	55.5	14.1	0.8	20.6
5	Ir-ReO_x/SiO_2 + Ru(5)/SiO_2	H^+/Ir = 1	32.0	15	47.7	18.4	24.0	4.5	5.4

Reaction conditions: glycerol 4 g, H_2O 2 g, catalyst 150 mg, P_{H_2} = 8 MPa (at 393 K), H_2SO_4aq 0 or 1.5 mg (H^+/Ir = 1), T = 393 K, t = 4 h. Reduction conditions: P_{H_2} = 8 MPa (at 473 K), T = 473 K, t = 1 h. PrD: propanediol; PrOH: propanol; Others: ethyleneglycol + ethanol + propane + ethane + methane.

Please cite this article in press as: M. Tamura, et al., J. Mol. Catal. A: Chem. (2013), http://dx.doi.org/10.1016/j.molcata.2013.09.015

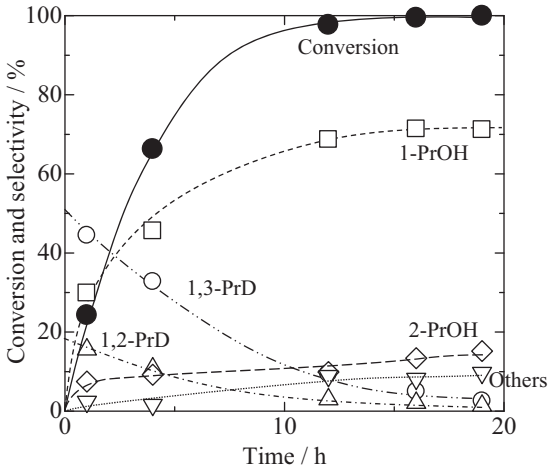

Fig. 1. Time-course profile of the glycerol hydrogenolysis over Ru(4.4)-Ir-ReO_x/SiO_2 (●: conversion; □: 1-propanol selectivity; ○: 1,3-propanediol selectivity; △: 1,2-propanediol selectivity; ◊: 2-propanol selectivity; ▽: others). Reaction conditions: glycerol 4 g, H_2O 2 g, P_{H_2} = 8 MPa (at 393 K), Ru(4.4)-Ir-ReO_x/SiO_2 150 mg, H_2SO_4aq 1.5 mg (H^+/Ir = 1), T = 393 K. PrD: propanediol; PrOH: propanol; Others: ethyleneglycol + ethanol + propane + ethane + methane.

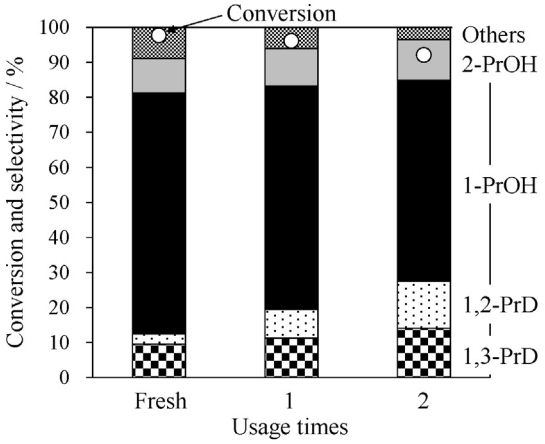

Fig. 2. Reuse of Ru(4.4)-Ir-ReO_x/SiO_2 in the glycerol hydrogenolysis. Reaction conditions: glycerol 4 g, H_2O 2 g, P_{H_2} = 8 MPa (at 393 K), Ru(4.4)-Ir-ReO_x/SiO_2 150 mg, H_2SO_4aq 1.5 mg (H^+/Ir = 1), T = 393 K, t = 12 h. PrD: propanediol; PrOH: propanol; Others: ethyleneglycol + ethanol + propane + ethane + methane.

entries 3 and 4). The conversion of the physically mixed catalyst was almost the same as the sum of those of Ir-ReO_x/SiO_2 and Ru(5)/SiO_2, which is much lower than that of Ru(4.4)-Ir-ReO_x/SiO_2. Along with the results in Table 3, these results show that coexistence of acid and Ru species with Ir-ReO_x/SiO_2 is effective to the increase of the activity.

The reaction time dependence of the glycerol hydrogenolysis over Ru(4.4)-Ir-ReO_x/SiO_2 is shown in Fig. 1. At the reaction time of 4 h, the yield of 1,3-PrD was high, and it decreased with increasing reaction time. On the other hand, the yields of 1-propanol and 2-propanol were gradually increased with increasing the reaction time, and at the reaction time of 12 h, the yields of these products were almost saturated. Maximum yield of 1-propanol was 71% at 16 h, and that of propanols (1-propanol + 2-propanol) was 86% at 19 h. These maximum yields of 1-propanol and propanols (1-propanol + 2-propanol) in the glycerol hydrogenolysis were slightly lower than those by the previous reported catalyst, Rh-ReO_x/SiO_2 (1-propanol: 76% and propanols (1-propanol + 2-propanol): 92% in 24 h) [45], however, the activity of Ru(4.4)-Ir-ReO_x/SiO_2 is higher than that of Rh-ReO_x/SiO_2.

To verify the stability of the catalyst, the Ru(4.4)-Ir-ReO_x/SiO_2 catalyst was used repeatedly, and the results are shown in Fig. 2. The significant loss of conversion and selectivity was not observed over the used catalyst. The XRD, XANES and EXAFS patterns of the recovered Ru(4.4)-Ir-ReO_x/SiO_2 were similar to those of the fresh Ru(4.4)-Ir-ReO_x/SiO_2 as shown below, indicating that the structure of Ru(4.4)-Ir-ReO_x/SiO_2 was maintained during the catalytic reaction and calcination treatment.

3.3. *Characterization of Ru-added Ir-ReO_x/SiO_2 catalyst and reaction mechanism*

To clarify the structure of Ru-added Ir-ReO_x/SiO_2, Ru(4.4)-Ir-ReO_x/SiO_2 catalyst was selected as a model catalyst. The profiles of temperature-programmed reduction (TPR) of Ru(5)/SiO_2, Ru(4.4)-Ir-ReO_x/SiO_2 and Ir-ReO_x/SiO_2 are shown in Fig. 3 and the result of the valence of Re was presented in Table 6. As reported previously [33], Ir-ReO_x/SiO_2 showed only one large peak (peak top = 469 K) (Fig. 3a). Ru(5)/SiO_2 showed two peaks between 400 and 475 K and no peak over 475 K (Fig. 3c), which indicates that Ru(5)/SiO_2 was completely reduced below 475 K. Total amount of consumed H_2, which was calculated using the total peak area of Ru(5)/SiO_2, corresponds to H_2 amount required for reduction of Ru^{4+}. This result suggests that the oxidation state of Ru of the calcined catalyst is RuO_2. On the other hand, Ru(4.4)-Ir-ReO_x/SiO_2 showed the broad signal between 372 and 475 K (Fig. 3b), which is almost the same reduction temperature as that of Ru(5)/SiO_2 and is lower reduction temperature than that of Ir-ReO_x/SiO_2. This result suggests that presence of Ru promoted the reduction of Ir-ReO_x/SiO_2. Assuming that the oxidation states of Ir and Ru of the calcined catalyst were Ir^{4+} [33,34,39] and Ru^{4+}, the peak area of the TPR profile of Ru(4.4)-Ir-ReO_x/SiO_2 provided the result that the valence of Re was changed to +4.8 from +7 in addition to the total reduction of Ir and Ru.

Fig. 4 shows XRD patterns of Ir-ReO_x/SiO_2 and Ru(5)/SiO_2 after the reduction, and Ru(4.4)-Ir-ReO_x/SiO_2 after the reduction and reaction. Ru(5)/SiO_2 showed peaks due to Ru metal as shown in Fig. 4d, where the average size of Ru metal is calculated to be 4.6 nm from the linewidth of the peak at around 44°. As reported previously [33], the main peak position of Ir-ReO_x/SiO_2 after the reduction at 473 K was $2\theta = 41°$ (Fig. 4a), which was assigned to Ir metal because the peak position was almost the same as that on Ir/SiO_2. The peaks corresponding to Re metal or ReO_x were not detected at all, indicating that Re species was highly dispersed. As for Ru(4.4)-Ir-ReO_x/SiO_2 catalyst after the reduction (Fig. 4b),

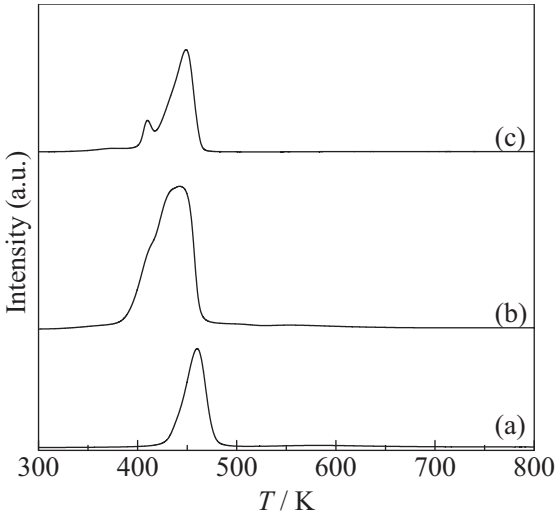

Fig. 3. TPR profiles of various catalysts: (a) Ir-ReO_x/SiO_2, (b) Ru(4.4)-Ir-ReO_x/SiO_2 and (c) Ru(5)/SiO_2.

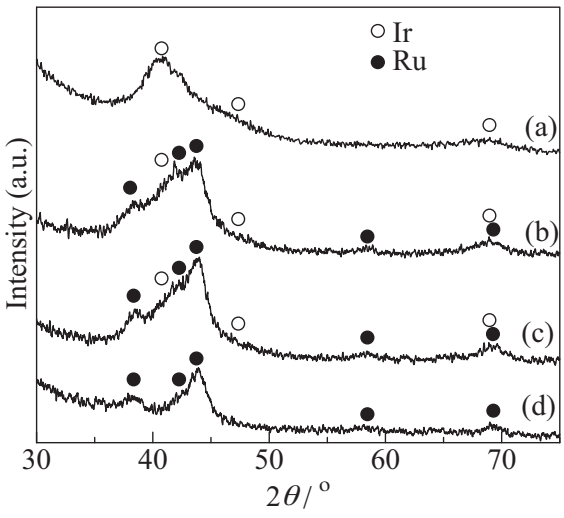

Fig. 4. XRD patterns of catalysts. (a) Ir-ReO_x/SiO_2 after the reduction treatment, (b) Ru(4.4)-Ir-ReO_x/SiO_2 after the reduction treatment, (c) Ru(4.4)-Ir-ReO_x/SiO_2 after the reaction and (d) Ru(5)/SiO_2 after the reduction treatment.

broad signals were observed at the region between 40° and 48°. The characteristic peaks assignable to Ru metal were observed at 38.4° and 58.3°, which indicates that Ru metal exists on the Ru(4.4)-Ir-ReO_x/SiO_2 catalyst. However, the particle sizes of Ru and Ir could not be estimated because of the overlap of the peaks. On the other hand, the pattern of the used Ru(4.4)-Ir-ReO_x/SiO_2 (Fig. 4c) was similar to those of fresh Ru(4.4)-Ir-ReO_x/SiO_2 catalyst after the reduction, which suggests that the structure of Ru(4.4)-Ir-ReO_x/SiO_2 was maintained during the reaction.

The results of the Ir L_3-edge EXAFS measurements of Ir-ReO_x/SiO_2 after the reaction, Ru(4.4)-Ir-ReO_x/SiO_2 after the reduction and the catalytic use, and Ir powder were shown in Fig. 5 and Table 5. From the curve fitting analysis of reduced Ru(4.4)-Ir-ReO_x/SiO_2, Ir was in metallic state, and the presence of Ir-Ir (or -Re) bond was observed, however, that of the Ir-Ru bond was not observed, which suggests no interaction between Ir and Ru of Ru(4.4)-Ir-ReO_x/SiO_2. Ir-Ir (or -Re) bond length and the coordination number (CN) on Ru(4.4)-Ir-ReO_x/SiO_2 were 0.276 nm and 10.4, respectively. The CN is comparable to that of Ir-ReO_x/SiO_2, suggesting that Ir metal particle size of Ru(4.4)-Ir-ReO_x/SiO_2 is almost the same as that of Ir-ReO_x/SiO_2. The results of

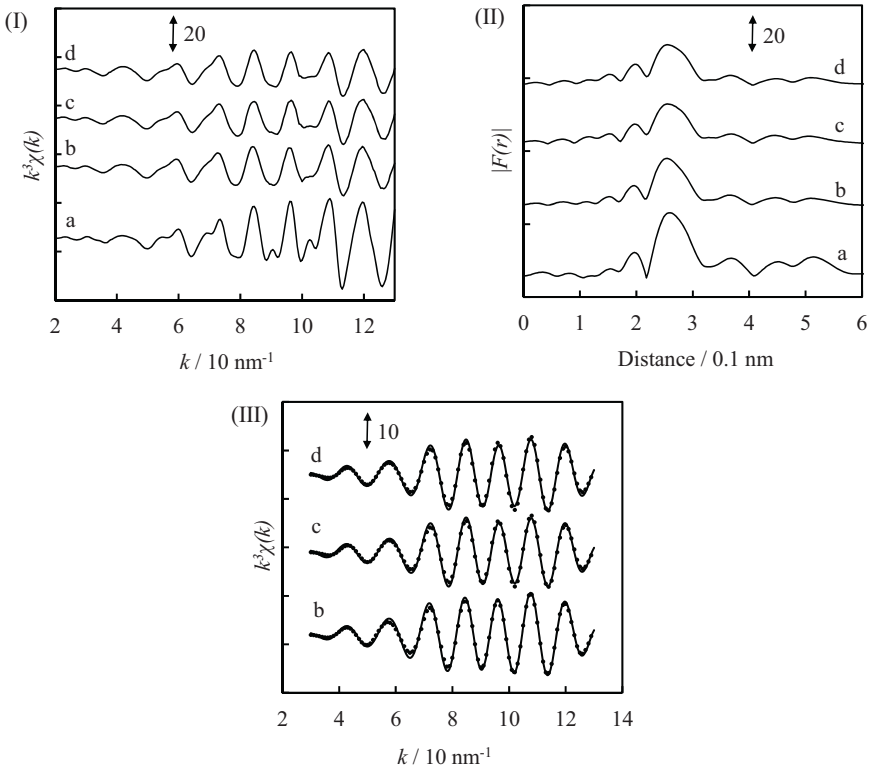

Fig. 5. Results of Ir L_3-edge EXAFS analysis of Ir-ReO_x/SiO_2 and Ru(4.4)-Ir-ReO_x/SiO_2. (I) k^3-Weighted EXAFS oscillations. (II) Fourier transform of k^3-weighted Ir L_3-edge EXAFS, FT range: 30–130 nm^{-1}. (III) Fourier filtered EXAFS data (solid line) and calculated data (dotted line), Fourier filtering range: 0.166–0.325 nm. (a) Ir powder, (b) Ir-ReO_x/SiO_2 after the catalytic use, (c) Ru(4.4)-Ir-ReO_x/SiO_2 after the reduction and (d) Ru(4.4)-Ir-ReO_x/SiO_2 after the catalytic use.

Table 5
Curve fitting results of Ir L_3-edge EXAFS of Ir-ReO_x/SiO_2 and Ru(4.4)-Ir-ReO_x/SiO_2.

Catalyst	State	Shells	CN[a]	R ($\times10^{-1}$ nm)[b]	σ ($\times10^{-1}$ nm)[c]	ΔE_0 (eV)[d]	R_f (%)[e]
Ir-ReO_x/SiO_2	Reaction	Ir—Ir (or —Re)	10.6 ± 0.6	2.76 ± 0.01	0.071 ± 0.003	−1.6 ± 0.9	1.0
Ru(4.4)-Ir-ReO_x/SiO_2	Reduction	Ir—Ir (or —Re)	10.4 ± 0.6	2.76 ± 0.01	0.074 ± 0.003	−0.4 ± 1.0	1.4
Ru(4.4)-Ir-ReO_x/SiO_2	Reaction	Ir—Ir (or —Re)	10.5 ± 0.7	2.76 ± 0.01	0.073 ± 0.003	−0.5 ± 1.0	1.5
Ir powder		Ir—Ir	12	2.77	0.060	0.0	–

[a] Coordination number.
[b] Bond distance.
[c] Debye–Waller factor.
[d] Difference in the origin of photoelectron energy between the reference and the sample.
[e] Residual factor. Fourier filtering range: 0.166–0.325 nm.

Please cite this article in press as: M. Tamura, et al., J. Mol. Catal. A: Chem. (2013), http://dx.doi.org/10.1016/j.molcata.2013.09.015

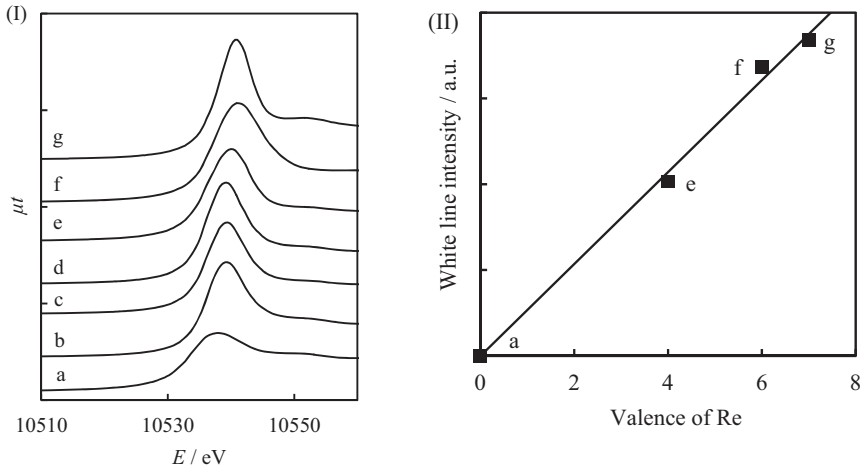

Fig. 6. Results of Re L_3-edge XANES analysis of Ir-ReO_x/SiO_2 and Ru(4.4)-Ir-ReO_x/SiO_2. (I) Re L_3-edge XANES spectra. (II) Relation between white line area and valence of Re. (a) Re powder, (b) Ir-ReO_x/SiO_2 after the catalytic use, (c) Ru(4.4)-Ir-ReO_x/SiO_2 after the reduction, (d) Ru(4.4)-Ir-ReO_x/SiO_2 after the catalytic use, (e) ReO_2, (f) ReO_3 and (g) Re_2O_7.

Ru(4.4)-Ir-ReO_x/SiO_2 after the reaction were in accordance with those of Ru(4.4)-Ir-ReO_x/SiO_2 after the reduction, which indicates that state of Ir maintains during the reaction.

Fig. 6 shows the Re L_3-XANES spectra of Ru(4.4)-Ir-ReO_x/SiO_2 and reference compounds, and the relation between white line area and valence of Re. We have previously reported that the average valence of Re species can be estimated by examining the white line area in the XANES spectra [64–66]. In the cases of Ir-ReO_x/SiO_2 after the catalytic use, the average valence of Re was determined to be +3.1 (Table 6), which agreed with +3.1 of Re of reduced Ir-ReO_x/SiO_2 reported previously [34]. For Ru(4.4)-Ir-ReO_x/SiO_2 after the reduction, the average valence of Re was +4.1 and the used Ru(4.4)-Ir-ReO_x/SiO_2 also provided the same average valence of Re (+4.0). These average valences of Re seem to be a little lower than that calculated from TPR (+4.8). The tendency that the average valence of Re calculated from TPR is a little higher that calculated from XANES on Ru(4.4)-Ir-ReO_x/SiO_2 was observed in case of Ir-ReO_x/SiO_2 (Table 6). The difference in the valence from the XANES analysis and TPR can be explained by the difference of pretreatment conditions between $P_{H_2} = 8$ MPa in water in XANES/EXAFS measurement and $P_{H_2} = 0.05$ atm in N_2 flow in TPR. Similar tendency in the valence difference was also observed in the cases of Rh-ReO_x/SiO_2 [24], Ir-ReO_x/SiO_2 [34] and Pt-ReO_x/SiO_2 [64,65]. On the other hand, the average valence of Re for Ru(4.4)-Ir-ReO_x/SiO_2 catalyst was higher than that of Ir-ReO_x/SiO_2, suggesting that addition of Ru species changes the state of ReO_x species.

Fig. 7 shows the results of Re L_3-edge EXAFS analysis of Ir-ReO_x/SiO_2 after the reaction, Ru(4.4)-Ir-ReO_x/SiO_2 after the reduction and the catalytic use, and reference compounds. Table 7 summarizes the curve fitting results. The curve fitting analysis of reduced Ru(4.4)-Ir-ReO_x/SiO_2 indicates the presence of the Re-O, Re-Ir (or -Re) and Re-Ru bonds with bond length (R) of 0.201, 0.266 and 0.265 nm, respectively, and coordination number (CN) of 3.0, 5.0 and 0.8, respectively. These results were the same as those of Ru(4.4)-Ir-ReO_x/SiO_2 after the reaction within the error range. If the curve fitting was carried out without Re-Ru bond, the fitting was much worse than that with Re-Ru bond (Table S1 and Fig. S2), which strongly supports the existence of Re-Ru bond. No change of the valence of Re suggests the state of ReO_x species was maintained during the reaction. An important point is that the presence of Re-Ru bond indicates that the interaction between ReO_x species and Ru species exists. Compared with the results of Ir-ReO_x/SiO_2, CN of Re-O of Ru(4.4)-Ir-ReO_x/SiO_2 is larger than that of Ir-ReO_x/SiO_2, which can be explained well by the higher oxidation state of Re over Ru(4.4)-Ir-ReO_x/SiO_2 than that over Ir-ReO_x/SiO_2, suggesting that Re interacted with Ru has higher oxidation state than that with Ir.

Table 6
The average valence of the Re species estimated by the results of Re L_3-edge XANES and TPR analysis of Ir-ReO_x/SiO_2 and Ru(4.4)-Ir-ReO_x/SiO_2.

Catalyst	State	Valence of Re	
		XANES	TPR
Ir-ReO_x/SiO_2	Reaction	3.1	4.5
Ru(4.4)-Ir-ReO_x/SiO_2	Reduction	4.1	4.8
Ru(4.4)-Ir-ReO_x/SiO_2	Reaction	4.0	–

Fig. 8 shows the Ru K-edge EXAFS spectra of the used catalysts and reference compounds. The results were summarized in Table 8. The curve fitting analysis of Ru(4.4)-Ir-ReO_x/SiO_2 after reduction showed that Ru was in metallic state. The presence of the Ru-Ru bond and Ru-Re (or -Ir) bond was verified. Considering the results of Ir L_3-edge EXAFS and Re L_3-edge EXAFS of Ru(4.4)-Ir-ReO_x/SiO_2, Ru-Re (or -Ir) bond can be mainly derived from Ru-Re bond. The curve fitting analysis of Ru(4.4)-Ir-ReO_x/SiO_2 after the reaction was almost the same as that of reduced Ru(4.4)-Ir-ReO_x/SiO_2, which indicates that the state of Ru is not influenced by the reaction. The CN of Re-Ru on Ru(4.4)-Ir-ReO_x/SiO_2 was 0.8, which agrees well with that of Ru-Re (0.8) (Table 7). Considering that the molar ratio Re/Ru is equivalent to be 1.1, this accordance of these CNs is quite valid. On the other hand, the distance of the reported Ru-Re bond was 0.265 nm (Tables 7 and 8) and this is shorter than that of Ru-Re alloy (0.269 nm, molar ratio of Re/Ru = 0.54/0.46) [67], suggesting the existence of cationic species between Ru and Re species. This interpretation is also supported by the structural analysis of Rh-ReO_x catalysts [37,68–70]. Since Ru species is in metallic state as shown in the results of TPR and EXAFS, Re species on Ru is also in cationic state, probably ReO_x species like the case of ReO_x species on Ir. Based on the above results on the structural analysis, Ir metal and Ru metal of Ru(4.4)-Ir-ReO_x/SiO_2 exist separately, and ReO_x species are located on both Ir and Ru metals, in that Ir-ReO_x species and Ru-ReO_x species can be formed separately on SiO_2. Taking CN of Ir-Ir (or -Re), Re-Ir bonds and oxidation state of Re of Ru(4.4)-Ir-ReO_x/SiO_2 into account, the structure of Ir-ReO_x species on Ru(4.4)-Ir-ReO_x/SiO_2 will be similar to that of Ir-ReO_x/SiO_2, which is reported as follows:

Please cite this article in press as: M. Tamura, et al., J. Mol. Catal. A: Chem. (2013), http://dx.doi.org/10.1016/j.molcata.2013.09.015

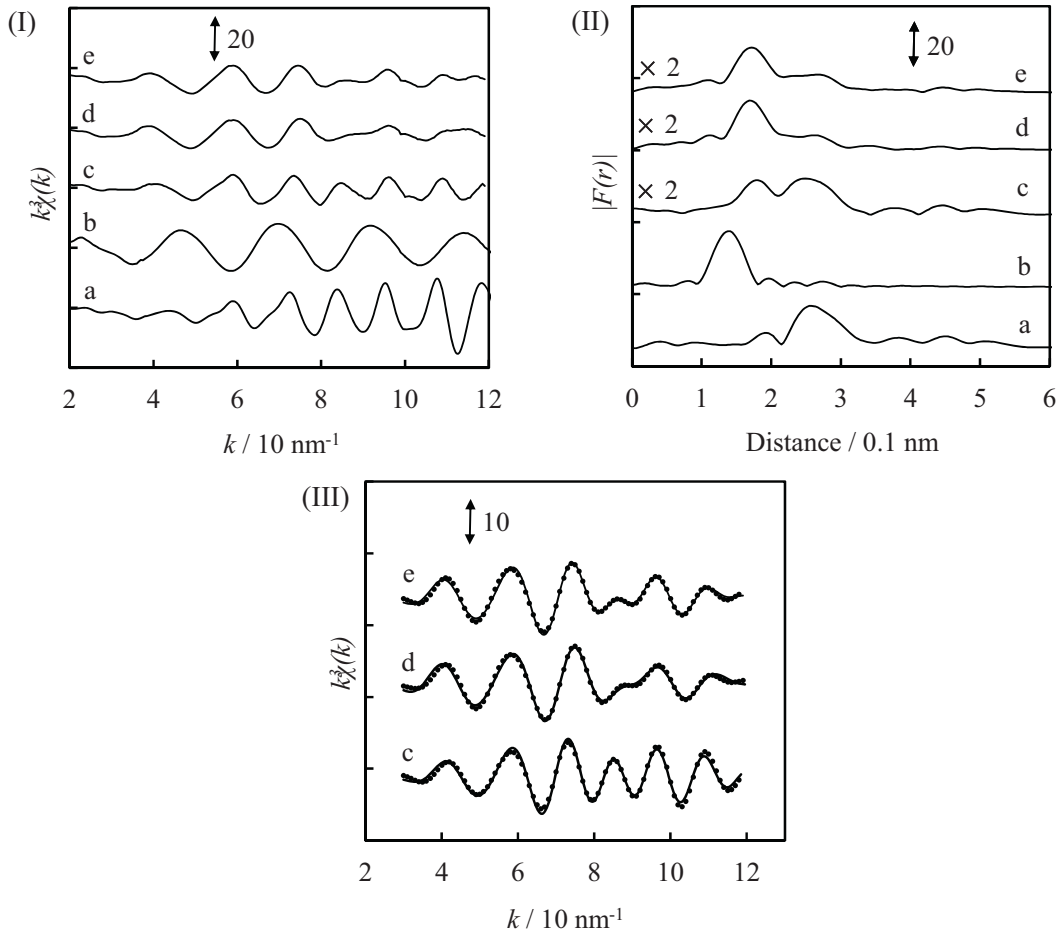

Fig. 7. Results of Re L_3-edge EXAFS analysis of Ir-ReO_x/SiO_2 and Ru(4.4)-Ir-ReO_x/SiO_2. (I) k^3-Weighted EXAFS oscillations. (II) Fourier transform of k^3-weighted Re L_3-edge EXAFS, FT range: 30–120 nm^{-1}. (III) Fourier filtered EXAFS data (solid line) and calculated data (dotted line), Fourier filtering range: 0.129–0.316 nm. (a) Re powder, (b) NH_4ReO_4, (c) Ir-ReO_x/SiO_2 after the catalytic use, (d) Ru(4.4)-Ir-ReO_x/SiO_2 after the reduction and (e) Ru(4.4)-Ir-ReO_x/SiO_2 after the catalytic use.

supported Ir is in the metallic state and the Re species form low-valent oxide clusters (ReO_x) that partially cover the Ir metal surface [33,34,39].

The amount of CO adsorption on the reduced catalysts was measured. The adsorption amount of CO on the Ir sites of Ir-ReO_x/SiO_2 catalyst was be 0.032 mmol g$_{\text{-cat}}^{-1}$. On the other hand, the adsorption amount of CO on Ru(4.4)-Ir-ReO_x/SiO_2 catalyst was determined to be 0.092 mmol g$_{\text{-cat}}^{-1}$. As the state of Ir in Ru(4.4)-Ir-ReO_x/SiO_2 was almost the same as that in Ir-ReO_x/SiO_2 from the results of XAFS, the amount of CO adsorption on the Ru sites is calculated to be about 0.060 mmol g$_{\text{-cat}}^{-1}$. Here, it is assumed that Ru metal size of Ru(4.4)-Ir-ReO_x/SiO_2 is the same as that of Ru(5)/SiO_2 (4.6 nm) as suggested from XRD patterns (Figs. 4b and d). The number of the outer layer of Ru metal particles is calculated to 0.12 mmol g$_{\text{-cat}}^{-1}$, which is determined according to the established method [71] by using the atomic diameter of Ru (0.266 nm) and assuming that Ru particles have a cubo-octahedral shape. This value (0.12 mmol g$_{\text{-cat}}^{-1}$) is larger than the observed amount of

Table 7
Curve fitting results of Re L_3-edge EXAFS of Ir-ReO_x/SiO_2 and Ru(4.4)-Ir-ReO_x/SiO_2.

Catalyst	State	Shells	CN[a]	R ($\times10^{-1}$ nm)[b]	σ ($\times10^{-1}$ nm)[c]	ΔE_0 (eV)[d]	R_f (%)[e]
Ir-ReO_x/SiO_2	Reaction	Re—O	1.7 ± 0.3	2.03 ± 0.02	0.080 ± 0.013	−0.6 ± 3.0	2.1
		Re—Ir (or —Re)	6.1 ± 0.7	2.68 ± 0.01	0.082 ± 0.003	8.1 ± 1.2	
Ru(4.4)-Ir-ReO_x/SiO_2	Reduction	Re—O	3.0 ± 0.4	2.01 ± 0.01	0.076 ± 0.006	−3.6 ± 2.2	2.1
		Re—Ir (or —Re)	5.0 ± 0.5	2.66 ± 0.01	0.089 ± 0.003	8.8 ± 1.8	
		Re—Ru	0.8 ± 0.2	2.65 ± 0.02	0.065 ± 0.010	9.9 ± 3.7	
Ru(4.4)-Ir-ReO_x/SiO_2	Reaction	Re—O	2.8 ± 0.3	2.02 ± 0.01	0.077 ± 0.006	−2.1 ± 1.4	1.8
		Re—Ir (or —Re)	5.1 ± 0.5	2.67 ± 0.01	0.088 ± 0.004	8.4 ± 1.8	
		Re—Ru	0.7 ± 0.3	2.65 ± 0.02	0.066 ± 0.014	8.2 ± 1.7	
NH_4ReO_4	–	Re=O	4	1.73	0.060	0.0	–

[a] Coordination number.
[b] Bond distance.
[c] Debye–Waller factor.
[d] Difference in the origin of photoelectron energy between the reference and the sample.
[e] Residual factor. Fourier filtering range: 0.129–0.316 nm.

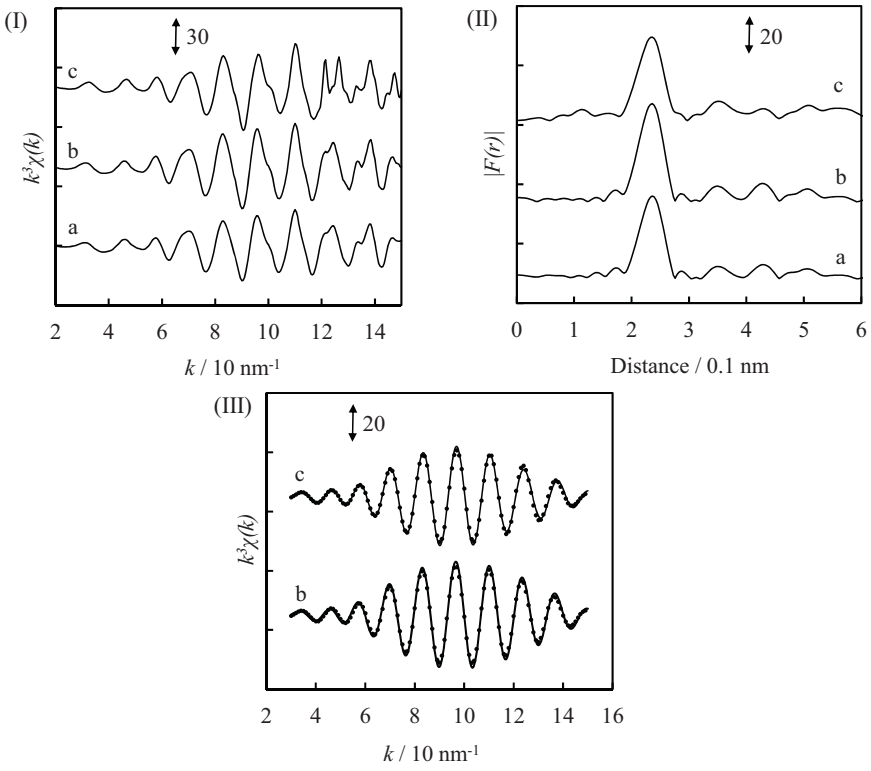

Fig. 8. Results of Ru *K*-edge EXAFS analysis of Ru(4.4)-Ir-ReO_x/SiO_2. (I) k^3-Weighted EXAFS oscillations. (II) Fourier transform of k^3-weighted Ru *K*-edge EXAFS, FT range: 30–150 nm^{-1}. (III) Fourier filtered EXAFS data (solid line) and calculated data (dotted line), Fourier filtering range: 0.166–0.325 nm. (a) Ru powder, (b) Ru(4.4)-Ir-ReO_x/SiO_2 after the reduction and (c) Ru(4.4)-Ir-ReO_x/SiO_2 after the catalytic use.

Table 8
Curve fitting results of Ru *K*-edge EXAFS of Ru(4.4)-Ir-ReO_x/SiO_2.

Catalyst	State	Shells	CN[a]	R ($\times10^{-1}$ nm)[b]	σ ($\times10^{-1}$ nm)[c]	ΔE_0 (eV)[d]	R_f (%)[e]
Ru(4.4)-Ir-ReO_x/SiO_2	Reduction	Ru—Ru	10.2 ± 0.3	2.66 ± 0.01	0.070 ± 0.001	1.6 ± 1.1	1.1
		Ru—Re	0.8 ± 0.5	2.65 ± 0.09	0.071 ± 0.011	1.5 ± 8.9	
Ru(4.4)-Ir-ReO_x/SiO_2	Reaction	Ru—Ru	10.1 ± 0.5	2.65 ± 0.01	0.071 ± 0.002	1.8 ± 1.0	0.9
		Ru—Re	0.8 ± 0.6	2.65 ± 0.05	0.071 ± 0.021	1.3 ± 10.3	
Rh foil	–	Rh—Rh	12	2.68	0.060	0.0	–

[a] Coordination number.
[b] Bond distance.
[c] Debye–Waller factor.
[d] Difference in the origin of photoelectron energy between the reference and the sample.
[e] Residual factor. Fourier filtering range: 0.166–0.325 nm.

CO adsorption on the Ru sites (0.06 mmol $g_{\text{-cat}}^{-1}$). Therefore, it is thought that Ru metal is partially covered with ReO_x species, as supported by the EXAFS results.

From these results, the proposed catalyst model and reaction mechanism are shown in Scheme 2. High performance of Ru(4.4)-Ir-ReO_x/SiO_2 will be derived from the combination of Ru-ReO_x species and Ir-ReO_x species. The high selectivity to 1,3-propanediol over Ru-Ir-ReO_x/SiO_2 catalysts implies that the main active species

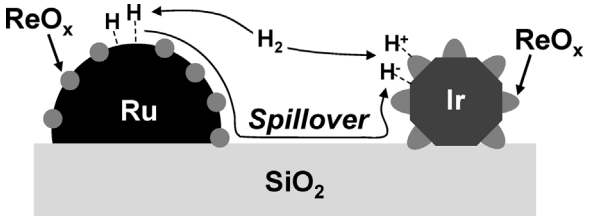

Scheme 2. The proposed catalyst and reaction model.

of the catalyst is Ir-ReO_x species. As shown in Tables 3 and 4, Ru/SiO_2 catalyst had low activity in the hydrogenolysis of glycerol [22,34], and mainly affords 1,2-propanediol or ethyleneglycol, which is derived from C-C clacking on Ru species. In addition, Re-added Ru catalysts also showed similar tendency [34,72,73]. Therefore, it is concluded that Ru-ReO_x species on Ru-Ir-ReO_x/SiO_2 mainly works as an enhancer of the activity of Ir-ReO_x species. Our previous reports have indicated that the active species in the glycerol hydrogenolysis over Ir-ReO_x/SiO_2 catalysts is hydride species adsorbed on the interface between Ir metal and ReO_x clusters, and the coverage of the hydride species is very low judging from the reaction order (~1) with respect to hydrogen pressure in the gas phase [33,34,38,43]. Therefore, the increase of the active hydrogen species should be connected to the enhancement of the activity of Ir-ReO_x. On the Ru-Ir-ReO_x/SiO_2 catalysts, Ru species as a promoter does not interact directly with the catalytically active Ir-ReO_x species, therefore, it is thought that Ru has a remote activation potential of Ir-ReO_x species. One interpretation is the hydrogen spillover effect. As reported previously [74–76], hydrogen species

dissociates on the metal surface and they spill over to the support surface and neighboring oxides to form proton [74] and hydride [75,76]. In general, Ru can homolytically dissociate H_2 to two H species and the H species generated on Ru-ReO_x species of Ru-Ir-ReO_x/SiO_2 can spill over onto Ir-ReO_x species to increase active H species on Ir-ReO_x species, leading to the high activity of Ru-Ir-ReO_x/SiO_2 (Scheme 2).

4. Conclusions

Ru-added Ir-ReO_x/SiO_2 catalyst showed high activity for the hydrogenolysis of glycerol to 1,3-propanediol or 1-propanol. In particular, Ru(0.9)-Ir-ReO_x/SiO_2 showed higher activity (2–3 times) than Ir-ReO_x/SiO_2 with high selectivity to 1,3-propanediol comparable to Ir-ReO_x/SiO_2. In addition, Ru(4.4)-Ir-ReO_x/SiO_2 showed very high activity for the hydrogenolysis of glycerol to 1-propanol, and 71% yield of 1-propanol and 84% yield of propanols (1-propanol and 2-propanol) were achieved. Based on TPR, XRD, XAFS and CO adsorption, the catalyst model of Ru(4.4)-Ir-ReO_x/SiO_2 was proposed. Ir and Ru metals were partially covered by ReO_x species, and Ir-ReO_x and Ru-ReO_x separately exist on SiO_2. The main active sites are on Ir-ReO_x of Ru(4.4)-Ir-ReO_x/SiO_2. High performance of Ru-Ir-ReO_x/SiO_2 is derived from the increase of active species on Ir-ReO_x by spillover of H species generated on Ru-ReO_x.

Acknowledgment

A part of this work is founded by the Cabinet Office, Government of Japan, through its “Funding Program for Next Generation World-Leading Researchers”.

Appendix A. Supplementary data

Supplementary data associated with this article can be found, in the online version, at http://dx.doi.org/10.1016/j.molcata.2013.09.015.

References

[1] A. Corma, S. Iborra, A. Velty, Chem. Rev. 107 (2007) 2411–2502.
[2] P. Gallezot, Green Chem. 9 (2007) 295–302.
[3] M. Schlaf, Dalton Trans. (2006) 4645–4653.
[4] R.M. West, E.L. Kunkes, D.A. Simonetti, J.A. Dumesic, Catal. Today 147 (2009) 115–125.
[5] C.H. Zhou, J.N. Beltramini, Y.X. Fan, G.Q. Lu, Chem. Soc. Rev. 37 (2008) 527–549.
[6] M. Pagliaro, R. Ciriminna, H. Kimura, M. Rossi, C.D. Pina, Angew. Chem. Int. Ed. 46 (2007) 4434–4440.
[7] Y. Nakagawa, K. Tomishige, Catal. Sci. Technol. 1 (2011) 179–190.
[8] S. Hirasawa, H. Watanabe, T. Kizuka, Y. Nakagawa, K. Tomishige, J. Catal. 300 (2013) 205–216.
[9] C. Liang, Z. Ma, L. Ding, J. Qiu, Catal. Lett. 130 (2009) 169–176.
[10] M.A. Dasari, P. Kiatsimkul, W.R. Sutterlin, G.J. Suppes, Appl. Catal. A 281 (2005) 225–231.
[11] L. Huang, Y. Zhu, H. Zheng, Y. Li, Z. Zeng, J. Chem. Technol. Biotechnol. 83 (2008) 1670–1675.
[12] M. Balaraju, V. Rekha, P.S.S. Prasad, R.B.N. Prasad, N. Lingaiah, Catal. Lett. 126 (2008) 119–124.
[13] L.C. Meher, R. Gopinath, S.N. Naik, A.K. Dalai, Ind. Eng. Chem. Res. 48 (2009) 1840–1846.
[14] S. Wang, H. Liu, Catal. Lett. 117 (2007) 62–67.
[15] A. Perosa, P. Tundo, Ind. Eng. Chem. Res. 44 (2005) 8535–8537.
[16] T. Jiang, Y. Zhou, S. Liang, H. Liu, B. Han, Green. Chem. 11 (2009) 1000–1006.
[17] J. Wang, S. Shen, B. Li, H. Lin, Y. Yuan, Chem. Lett. 38 (2009) 572–573.
[18] Y. Kusunoki, T. Miyazawa, K. Kunimori, K. Tomishige, Catal. Commun. 6 (2005) 645–649.
[19] T. Miyazawa, Y. Kusunoki, K. Kunimori, K. Tomishige, J. Catal. 240 (2006) 213–221.
[20] T. Miyazawa, S. Koso, K. Kunimori, K. Tomishige, Appl. Catal. A 318 (2007) 244–251.
[21] T. Miyazawa, S. Koso, K. Kunimori, K. Tomishige, Appl. Catal. A 329 (2007) 30–35.
[22] I. Furikado, T. Miyazawa, S. Koso, A. Shimao, K. Kunimori, K. Tomishige, Green. Chem. 9 (2007) 582–588.
[23] A. Shimao, S. Koso, N. Ueda, Y. Shinmi, I. Furikado, K. Tomishige, Chem. Lett. 38 (2009) 540–541.
[24] Y. Shinmi, S. Koso, T. Kubota, Y. Nakagawa, K. Tomishige, Appl. Catal. B 94 (2010) 318–326.
[25] Z. Yuan, P. Wu, J. Gao, X. Lu, Z. Hou, X. Zheng, Catal. Lett. 130 (2009) 261–265.
[26] J. Chaminand, L. Djakovitch, P. Gallezot, P. Marion, C. Pinel, C. Rosier, Green Chem. 6 (2004) 359–361.
[27] N. Suzuki, Y. Yoshikawa, M. Takahashi, M. Tamura, WO Patent 2007129560 (2007).
[28] T. Kurosaka, H. Maruyama, I. Naribayashi, Y. Sasaki, Catal. Commun. 9 (2008) 1360–1363.
[29] L. Huang, Y. Zhu, H. Zheng, G. Dong, Y. Li, Catal. Lett. 131 (2009) 312–320.
[30] L.-Z. Qin, M.-J. Song, C.-L. Chen, Green Chem. 12 (2010) 1466–1472.
[31] O.M. Daniel, A. DeLaRiva, E.L. Kunkes, A.K. datye, J.A. Dumesic, R.J. Davis, ChemCatChem 2 (2010) 1107–1114.
[32] L. Gong, Y. Lu, Y. Ding, R. Lin, J. Li, W. Dong, T. Wang, W. Chen, Appl. Catal. A 390 (2010) 119–126.
[33] Y. Nakagawa, Y. Shinmi, S. Koso, K. Tomishige, J. Catal. 272 (2010) 191–194.
[34] Y. Amada, Y. Shinmi, S. Koso, T. Kubota, Y. Nakagawa, K. Tomishige, Appl. Catal. B 105 (2011) 117–127.
[35] J. Oh, S. Dash, H. Lee, Green Chem. 13 (2011) 2004–2007.
[36] S. Zhu, Y. Zhu, S. Hao, L. Chen, B. Zhang, Y. Li, Catal. Lett. 142 (2012) 267–274.
[37] S. Koso, H. Watanabe, K. Okumura, Y. Nakagawa, K. Tomishige, Appl. Catal. B 111–112 (2012) 27–37.
[38] Y. Nakagawa, X. Ning, Y. Amada, K. Tomishige, Appl. Catal. A 433–434 (2012) 128–134.
[39] Y. Amada, H. Watanabe, M. Tamura, Y. Nakagawa, K. Okumura, K. Tomishige, J. Phys. Chem. C 116 (2012) 23503–23514.
[40] T. Mizugaki, T. Yamakawa, R. Arundhathi, T. Mitsudome, K. Jitsukawa, K. Kaneda, Chem. Lett. 41 (2012) 1720–1722.
[41] J.t. Dam, K. Djanashvili, F. Kapteijn, U. Hanefeld, ChemCatChem 5 (2013) 497–505.
[42] M. Schlaf, P. Ghosh, P.J. Fagan, E. Hauptman, R.M. Bullock, Adv. Synth. Catal. 351 (2009) 789–800.
[43] K. Chen, K. Mori, H. Watanabe, Y. Nakagawa, K. Tomishige, J. Catal. 294 (2012) 171–183.
[44] R. Arundhathi, T. Mizugaki, T. Mitsudome, K. Jitsukawa, K. Kaneda, ChemSusChem 6 (2013) 1345–1347.
[45] Y. Amada, S. Koso, Y. Nakagawa, K. Tomishige, ChemSusChem 3 (2010) 728–736.
[46] K. Chen, M. Tamura, Z. Yuan, Y. Nakagawa, K. Tomishige, ChemSusChem 6 (2013) 613–621.
[47] H. Hattori, Top. Catal. 53 (2010) 432–438.
[48] C. Wang, H. Zhao, H. Wang, L. Liu, C. Xiao, D. Ma, Catal. Today 183 (2012) 143–153.
[49] M.K. Oudenhuijzen, J.A. van Bokhoven, J.T. Miller, D.E. Ramaker, D.C. Koningsberger, J. Am. Chem. Soc. 127 (2005) 1530–1540.
[50] Y. Yazawa, H. Yoshida, S. Komai, T. Hattori, Appl. Catal. A 233 (2002) 113–124.
[51] H. Yoshitake, Y. Iwasawa, J. Catal. 131 (1991) 276–284.
[52] J.K.A. Clarke, Chem. Rev. 75 (1975) 291–305.
[53] R. Ferrando, J. Jellinek, R. Johnston, Chem. Rev. 108 (2008) 845–910.
[54] D. Li, Y. Nakagawa, K. Tomishige, Appl. Catal. A 408 (2011) 1–24.
[55] D. Li, Y. Nakagawa, K. Tomishige, Chin. J. Catal. 33 (2012) 583–594.
[56] H. Tanaka, R. Kaino, Y. Nakagawa, K. Tomishige, Appl. Catal. A 378 (2010) 187–194.
[57] H. Tanaka, R. Kaino, K. Okumura, T. Kizuka, Y. Nakagawa, K. Tomishige, Appl. Catal. A 378 (2010) 175–186.
[58] S.R. Sashital, J.B. Cohen, R.L. Burwell, J.B. Butt Jr., J. Catal. 50 (1977) 479–493.
[59] J.W. Cook, D.E. Sayers, J. Appl. Phys. 52 (1981) 5024–5031.
[60] K. Okumura, J. Amano, N. Yasunobu, M. Niwa, J. Phys. Chem. B 104 (2000) 1050–1057.
[61] K. Okumura, S. Matsumoto, N. Nishiaki, M. Niwa, Appl. Catal. B 40 (2003) 151–159.
[62] A.L. Ankudinov, B. Ravel, J.J. Rehr, S.D. Conradson, Phys. Rev. B 58 (1998) 7565–7576.
[63] K. Tomishige, K. Asakura, Y. Iwasawa, J. Catal. 149 (1994) 70–80.
[64] T. Ebashi, Y. Ishida, Y. Nakagawa, S.-i. Ito, T. Kubota, K. Tomishige, J. Phys. Chem. C 114 (2010) 6518–6526.
[65] Y. Ishida, T. Ebashi, S. Ito, T. Kubota, K. Kunimori, K. Tomishige, Chem. Commun. (2009) 5308–5310.
[66] M. Ronning, T. Gjervan, R. Prestivik, D.G. Nicholson, A. Holmen, J. Catal. 204 (2001) 292–304.
[67] E. Rudy, B. Kieffer, H. Froehlich, Z. Metall. 53 (1962) 90–92.
[68] K. Chen, S. Koso, T. Kubota, Y. Nakagawa, K. Tomishige, ChemCatChem 2 (2010) 547–555.
[69] S. Koso, H. Watanabe, K. Okumura, Y. Nakagawa, K. Tomishige, J. Phys. Chem. C 116 (2012) 3079–3090.

[70] S. Koso, I. Furikado, A. Shimao, T. Miyazawa, K. Kunimori, K. Tomishige, Chem. Commun. (2009) 2035–2037.
[71] R. van Hardeveld, F. Hartog, Surf. Sci. 15 (1969) 189–230.
[72] L. Ma, D. He, Catal. Today 149 (2010) 148–156.
[73] G. Beamson, A.J. Papworth, C. Philipps, A.M. Smith, R. Whyman, J. Catal. 278 (2011) 228–238.
[74] K. Ebitani, J. Konishi, H. Hattori, J. Catal. 130 (1991) 257–267.
[75] K. Tomishige, A. Okabe, K. Fujimoto, Appl. Catal. A 194–195 (2000) 383–393.
[76] R. Ueda, T. Kusakari, K. Tomishige, K. Fujimoto, J. Catal. 194 (2000) 14–22.

Please cite this article in press as: M. Tamura, et al., J. Mol. Catal. A: Chem. (2013), http://dx.doi.org/10.1016/j.molcata.2013.09.015